DOI: 10.1002/fuce.201200065

On the Catalytic Degradation in Fuel Cell Power Supplies for Long-Life Mobile Field Sensors

J. Thangavelautham[1]*, S. Dubowsky[1]

[1] Field and Space Robotics Laboratory, Department of Mechanical Engineering, Massachusetts Institute of Technology, Cambridge, MA, USA

Received April 29, 2012; accepted November 15, 2012; published online December 07, 2012

Abstract

Important tasks such as environment monitoring require field devices such as sensors that can operate for long durations. Current power supply technologies such as batteries limit many applications. Fuel cells are a promising alternative to batteries because they can have much higher energy densities. However, their lives may be short due to catalyst degradation. Here, a simplified model of proton exchange membrane (PEM) fuel cell catalyst degradation is applied to small fuel cells. The model focuses on the combined effects of catalyst dissolution and migration. The effect of migration on catalyst degradation is found to be substantial and this has not been accounted for in previous models. The model considers the effect of field conditions such as varying power demands, temperature and humidity, and predicts the catalyst life of the fuel cell and its power output. The predicted life is a proposed metric that can quantify the relative importance and effect of field conditions on the catalyst particularly for the design and control of fuel cell power supplies. Experiments are presented that support the model. This model is applied to a study on field sensors and results suggests unless PEM fuel cells are isolated from damaging field conditions, they will have short lives.

Keywords: Catalyst Degradation, Field Sensors, Fuel Cells, Mobile Power

1 Introduction

Networks of sensor modules operating in unstructured outdoor environments have many important applications including environment monitoring in forestry, agriculture, disaster prediction (storm, earthquakes, tsunamis), energy (exploration, transportation, consumption) and border security [29]. These field sensor modules may be required to operate unattended for 3–5 years or more with only onboard power. Currently, such field devices use batteries or photovoltaics for power. Photovoltaics are not used often because they require large surface areas with good exposure to the sun [26]. As a result, batteries are most commonly used to power field systems. However, their lives are often limited by the total energy they can provide.

Conventional batteries provide high and variable power, but their total energy is limited due to their internal chemistry. For long life missions, they need to be recharged or replaced often. While significant work is being done to address their energy limitations [25], batteries currently cannot meet the high energy requirements of many long duration field sensors. Here, fuel cells are explored to meet these requirements.

Fuel cells have been suggested as a power source for field and mobile devices [32–35]. Fuel cells are electrochemical energy conversion devices that convert chemical energy directly into electricity. They can have high operating efficiencies and energy densities. In particular, proton exchange membrane (PEM) fuel cells are well suited for field devices, because of their high conversion efficiencies of 40–65% (LHV) [23, 24]. They operate at or near room temperature and produce clean exhaust. PEMs use hydrogen fuel and breathe oxygen to produce electricity [23, 24]. PEMs tend to have higher specific energy than the best current batteries.

However, PEM fuel cells face several challenges that limit their wide scale commercial adoption. First, PEM fuel cells are faced with low durability, due to degradation of its components, resulting in short lives [3, 9, 13–15, 46]. Although significant research and progress has been made in this field

[*] *Corresponding author, jekan@mit.edu*

over the past few years, hurdles remain for practical use. Second, the practical storage of hydrogen fuel using conventional methods is a challenge, due to low energy densities [41]. Third, PEM fuel cells have low power density and high cost compared to batteries [23]. The problem of hydrogen storage, low power densities and cost is being addressed by our research; however it is beyond the scope of this paper [22]. PEM fuel cells need to overcome limited durability due impart to catalyst degradation to attain wide scale use. Physical modeling of fuel cell catalyst degradation can be used to quantify the effect of operating conditions and enable better design and control of fuel cells so that they may overcome limited durability.

Current catalyst degradation models of fuel cells describe dissolution of the catalyst as the cause of catalyst degradation [13, 14]. These current models do not match well with experimental data and as a result it is not possible to make longer term predictions of fuel cell life and performance [13]. In this paper, a fuel cell catalyst degradation model is presented that expands on previous work [13, 14] and accounts for the effect of catalyst migration and dissolution on catalyst degradation. This phenomenon of catalyst migration as will be shown in this paper can have a substantial impact on catalyst degradation and cannot be ignored. Accounting for this phenomenon, the model better matches experimental data compared to previous models and is used to make life-time predictions of catalyst degradation under field conditions.

2 Background and Literature

It should be noted that important fundamental research is being done to develop more robust fuel cells which in time could enhance these devices for field applications. A PEM fuel cell membrane electrode assembly (MEA) has several major components that are all subject to degradation (Figure 1). They are the gas diffusion layer (GDL), the membrane and catalyst layers.

The GDL facilitates the transfer of the input gases to the anode and cathode. The anode catalyst layer facilitates the oxidation of hydrogen molecules into protons while the membrane allows for the transport of protons from the anode to the cathode. The cathode catalyst layer facilitates the assembly of protons and oxygen molecules into water via a reduction reaction. Extensive research has been done to identify the mechanisms that degrade these components and a brief overview of these mechanisms is presented in this section with a focus on catalyst degradation. The GDL degradation affects the ability of the cell to absorb reactants. This degradation includes loss of hydrophobicity of the cathode that results in flooding [17] causing loss in performance. Prolonged flooding is known to cause corrosion of various components of the fuel cell including the catalyst [46]. Structural damage, such as from freezing [10, 12], mechanical stress, wear and tear of a GDL can reduce the cell's ability to absorb fuel or oxidizer [3] and thus reducing a cell's performance and resulting in catalyst degradation. However, it should be noted that many of these sources of GDL degradation can be prevented by avoiding such conditions as structural damage, flooding, or freezing.

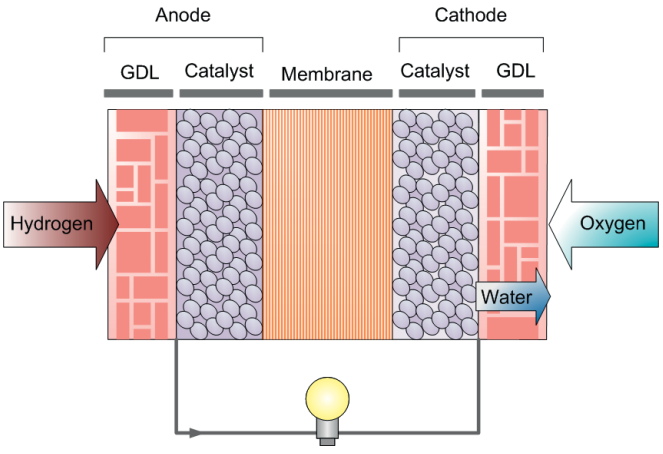

Fig. 1 A PEM fuel cell MEA and its major components.

Membranes are also subject to degradation and can be classified into three categories, thermal, mechanical, and chemical [1–3]. In addition, membranes can degrade due to migration of impurities, particularly catalyst particles that deposit in the membrane. This can result in local structural weak points that cause pinholes, permitting cross-over of reactant gases and their direct combustion of the reactants causing loss of power, rapid increase in temperature and fuel cell death [4]. The root cause of the above failure is the particles produced by catalyst degradation in the cathode.

Hence, in many cases platinum catalyst degradation in the cathode is an important factor in fuel cell durability and life [3, 13, 40]. One cause of catalyst degradation is the dissolution of the platinum particles into ions [3, 9, 13–15, 46]. The ions either redeposit on large platinum particles (similar to Ostwald ripening) or dissolve and migrate away from the catalyst layer and into nearby regions [37]. Sustained degradation reduces the available catalyst surface in the anode and cathode resulting in loss of power. It also weakens the carbon support structure that holds the platinum and vice-versa through corrosion of the carbon particles [8]. Carbon corrosion is another important source of degradation in a fuel cell [46]. The carbon structure breaks into particles that migrate into the membrane and GDL. The migrating platinum catalyst and carbon particles weakens the membrane structure as discussed above, causing irreversible structural damage ultimately resulting in tears and pinholes [6]. The fuel cell catalyst is impacted by the oxidation of the platinum particles [7]. Oxidation of the platinum particles results in the formation of surface films of platinum oxide that effectively reduces the available catalyst surface area resulting in loss of power. While oxidation of platinum reduces the surface area, it is also known to protect platinum particles beneath the oxide layer from dissolution.

Catalyst degradation in the cathode can be a major PEM degradation mechanism in many applications because it can

result in irreversible loss of power and cause structural failure of the membrane.

Extensive experimental evidence has shown that fuel cell catalyst degrades due to several operating factors including high operating voltages, high temperature, and high humidity [9, 11, 16]. Early empirical models attempted to capture the effect of catalyst degradation and the resultant power loss based on hours of operation [15]. These models are incomplete and do not account for the fuel cell operational factors that results in catalyst degradation. Several models of fuel cell electrochemical interactions account for platinum catalyst degradation [14, 13]. They capture the physics of the rate of dissolution and oxidation of the platinum particles. These models show the significant effect of fuel cell operating voltage on catalyst degradation [14, 13]. In these studies, the fuel cells are analyzed for conditions where the fuel cell's output voltage is varied in a square wave oscillating between 0.87 and 1.2 V. These conditions are intended to represent oscillatory voltage conditions relevant for PEM fuel cell powered automobiles [13]. It should be noted that voltage oscillation experiments has strong influence on the fuel cell cathode than the anode due to the slower reaction and reciprocal higher resistance of this electrode.

While the above studies have produced important results, the fuel cell condition that must be maintained for them to be practical long life power supplies for field conditions is still not well understood and is the focus of this paper.

3 Approach and Objective

Here, the development and experimental validation of a PEM fuel cell platinum catalyst degradation model is presented. This simplified model accounts for the physics of catalyst degradation of the cathode, including membrane conductivity, catalyst migration and dissolution and considers these effects on fuel cell catalyst life and power performance. The effects and interaction of the platinum with other important components of a fuel cell on catalyst degradation is accounted for, including the dependency of conductivity on the membrane and the effect of dissolution and migration of the catalyst particles into the membrane. The model accounts for field operating conditions, in particular operating voltage, temperature, and humidity. The model is applied to a field application, where the expected life and behavior of the fuel cell is predicted. Based on these results, the work suggests a set of design and control strategies to maximize catalyst life and operating efficiency of individual PEM fuel cell for field applications.

4 PEM Fuel Cell Catalyst Degradation Model

The PEM degradation model presented here is an extension of the models developed in [14] and [13] applied to small power supplies. The model accounts for the reduction of the total surface area of the catalyst in the cathode, where the catalyst layer is discretized into compartments, consisting of particles of catalyst. It considers the rate of platinum particle dissolution and oxidation. All of these reactions are dependent on the fuel cell operating conditions. Importantly, the model accounts for both dissolution and migration of the platinum particles, ignored in previous models. As will be shown later, accounting for migration of platinum particles can have a substantial impact on catalyst degradation. In addition, it can better explain published experiment results [13]. Oxidation of platinum is assumed to be affected by proton conductivity of the membrane due to the large electric field that in turn is dependent on its humidity, assuming a Nafion® membrane. These factors are not accounted for in previous models [14, 13]. Based on the rate of platinum dissolution and platinum oxidation, an updated number of platinum particles and catalyst surface area is obtained.

In this analysis, the cathode catalyst layer is assumed to contain platinum particles on a carbon support structure and is modeled as a one dimensional strip consisting of X grid squares of uniform thickness (Figure 2). The anode catalyst layer is not included in the model, because the cathode is more susceptible to degradation [14, 13].

The model assumes the platinum catalyst particles are spherical, uniformly distributed and can be categorized into two sizes, large particles with radius R_l and small particles with radius R_s. The total surface area of platinum particles is:

$$S = \sum_{x=1}^{X} \sum_{i=s,l} 4\pi N_{x,i} R_{x,i}^2 \tag{1}$$

where:

x is the grid position.

i is index small and large categories of particles.

$N_{x,i}$ is the number of platinum particles, in grid square x and of category i.

$R_{x,i}$ is the radius of the particles in grid square x and of category i.

The radius of the small and large platinum particles is expected to change due to dissolution of the platinum. The dissolution of the platinum occurs according to the following chemical reaction:

$$\mathrm{Pt} = \mathrm{Pt}^{2+} + 2e^- \tag{2}$$

where platinum breaks (dissolves) away from its lattice structure into ions. The dissolution potential of this reaction (i.e., spontaneously dissolves) is 1.188 V [38]. A second reaction occurs, when platinum is exposed to water molecules to form platinum oxide according to the following reaction:

$$\mathrm{Pt} + \mathrm{H_2O} \rightarrow \mathrm{PtO} + 2\mathrm{H}^+ + 2e^- \tag{3}$$

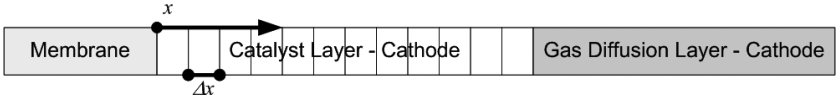

Fig. 2 Fuel cell catalyst layer coordinates.

The formation of platinum oxide on the platinum particles prevents further platinum from dissolving, but also reduces the effectiveness of the catalyst in disassembling the oxygen molecules and assembling water molecules. The potential for platinum oxidation (i.e. spontaneously oxidate) is 0.98 V [39]. Platinum oxide also dissolves away but this reaction is much slower than reactions given in (2) and (3) and is thus ignored [14].

The dissolution and oxidation of the platinum reduces the available active sites on the surface area for catalysis. The reactions of (2) and (3) are modeled by the Butler–Volmer rate equations given below based on [14, 13] but modified to include effects of humidity. These reactions determine the rate of production of platinum ions and platinum oxide, respectively:

$$r_{Pt^{2+}i} = k_{1a}\mathrm{RH}_a\theta_{iV}\left[\exp\left\{\frac{a_{1a}n_1F(V-U_{1i})}{RT}\right\} - \frac{c_{Pt^{2+}}}{c_{Pt^{2+}\mathrm{ref}}}\exp\left\{\frac{-a_{1c}n_1F(V-U_{1i})}{RT}\right\}\right] \quad (4)$$

and

$$r_{PtOi} = k_{2C}\mathrm{RH}_c\theta_i\exp\left\{\frac{a_{2a}n_2F(V-U_{2i})}{RT}\right\} - k_{2C}c_{H+}^2\theta_i\exp\left\{\frac{-a_{2c}n_2F(V-U_{2i})}{RT}\right\} \quad (5)$$

where:

i is the index of small and large categories of platinum particles.

k_{1a} is the platinum ion (Pt^{2+}) dissolution constant.

RH_a is the relative humidity of the anode.

RH_c is the relative humidity of the cathode.

θ is the oxide coverage of the catalyst surface.

θ_V is the vacant catalyst surface (i.e. not covered by oxide).

a_{1a} is the anodic transfer coefficient.

a_{1c} is the cathodic transfer coefficient.

n_1 is the equivalent number of electrons transferred per mole of Pt^{2+}.

n_2 is the equivalent number of electrons transferred per mole PtO.

F is Faraday's constant.

R is the universal gas constant.

V is the fuel cell operating voltage.

U_{1i} is the adjusted dissolution potential of Pt^{2+} [13]

U_{2i} is the adjusted dissolution potential of PtO [13].

T is the temperature.

c_{H+} is the relative proton activity.

c_{Pt2+} is the concentration of Pt^{2+}.

$c_{Pt2+\ \mathrm{ref}}$ is the reference concentration of Pt^{2+}.

As seen from these rate Eqs. (4) and (5), the dissolution and oxidation of the platinum is dependent on the operating voltage, temperature, and relative humidity. The rate of platinum oxidation is used to calculate the available platinum surface area. Oxidation of Pt according to Volmer–Butler rate equation is also a function of the proton activity. Oxidation is affected by the proton activity (c_{H+}), the ability for the protons to travel through the membrane due to the influence of an electric field. The available surface platinum molecules have an affinity to both the oxygen molecule and proton. Thus, with increased proton activity due to the large electrical field, there is a natural resistance to the formation of platinum oxide.

In the previous model, proton activity was taken as a constant [13], however here it is taken as a function of the relative humidity [14]:

$$c_{H+} = \frac{1}{\frac{EW}{\rho_{\mathrm{Nafion}}} + \lambda\frac{M_{H_2O}}{\rho_{H_2O}}} \quad (6)$$

where:

EW is the equivalent weight of the Nafion® ionomer.

ρ_{Nafion} is the density of Nafion®.

ρ_{H_2O} is the density of water.

M_{H_2O} is the molecular mass of water.

The water content of Nafion®, λ is a function of temperature and relative humidity and is given by the following [20]:

$$\lambda = C_0 + C_1\mathrm{RH} + C_2\mathrm{RH}^2 + C_3\mathrm{RH}^3 \quad (7)$$

where:

$$\rho_{\mathrm{Nafion}} = \frac{C_4 + C_5\lambda}{1 + C_6\lambda} \quad (8)$$

and where:

$C_0,\ldots,C_6$ are constants, the values listed in Appendix.

RH is relative humidity of the membrane and $RH = RH_a/2 + RH_c/2$, the average of the cathode and anode relative humidity [13].

The rate of change of platinum oxide surface area is a modification from [14] and excludes the dissolution of platinum oxide, because it is known occur much slower than reaction (2) or (3) [13]:

$$\frac{d\theta_i}{dt} = \left(\frac{r_{PtOi}}{\Gamma_{\max}}\right) - \left(\frac{2\theta_i}{r_{Pti}}\right)\frac{dr_{Pti}}{dt} \quad (9)$$

and where:

θ is the oxide coverage of the catalyst surface.

r_{PtO} is the rate of reaction platinum oxide.

r_{Pt} is the platinum particle radius.

$\Gamma_{\max}$ is the number of moles of active sites per unit area of platinum.

By calculating the rate of platinum dissolution, migration and oxidation, a mass balance on the platinum ions can be obtained:

$$\varepsilon_j\frac{\partial c}{\partial t} = (1+kd)\cdot D\varepsilon_j^{1.5}\frac{\partial^2 c}{\partial x^2} + \sum_{i=S,L}A_i r_{Pti} \quad (10)$$

where:

ε_j is the electrolyte volume fraction.

c is the concentration of platinum ions.

d is the migration coefficient.

D is the diffusion coefficient.

A_i is the interfacial surface area.

x is the grid position along the layer of platinum.

The diffusion coefficient is a function of the electrolyte volume fraction ε_j within region j and assumes:

$$\tau = \sqrt{\varepsilon} \tag{11}$$

where:

τ is tortuosity [13].

The ratio of platinum ions transport by migration to diffusion defined as k has been ignored in previous catalyst degradation models [13] due to the limited operating voltages considered. Here it is the following:

$$k = \frac{N_{\text{migr}}}{N_{\text{diff}}} \approx \frac{2FiR_{\text{FC}}}{\text{RT}} \tag{12}$$

Platinum ions from the cathode both diffuse and migrate into the membrane. The ratio of particles transported due to migration is influenced by the strength of the electrical field from the current, i and resistance, R_{FC}. The strength of the electric field is dependent on the fuel cell operating point and, R_{FC} is from [15]:

$$R_{\text{FC}} \approx \frac{k_a l[1 + k_b\left(\frac{i}{A}\right) + k_c\left(\frac{i}{A}\right)^{2.5}\left(\frac{T}{T_0}\right)^2]}{A[\kappa_0 + \kappa\left(\frac{S(t)}{S_0}\right) - k_d - k_e\left(\frac{i}{A}\right)\exp\left\{\beta\left(\frac{T-303}{T}\right)\right\}]} \tag{13}$$

and where:

A is the area of the fuel cell.

l is the membrane thickness.

$k_a, k_b, k_c, k_d, k_e, \kappa_0$, κ and β are constants (values listed in Appendix).

T is temperature.

i is the current.

S_0 is the initial surface area of the catalyst.

$S(t)$ is the surface area of the catalyst at time t.

A_i is the interfacial surface area given as follows:

$$A_i = \frac{4\pi R_i^2}{v} N_i \tag{14}$$

where v is the volume occupied by each particle. The total mass of platinum available for catalysis is the initial mass minus the amount that diffuses and migrates away over a period of time:

$$M(t) = M(t=0) + A(1+kd)\int_0^t \varepsilon_{\text{M}} D \left.\frac{\partial c}{\partial x}\right|_{x=L} \text{d}t \tag{15}$$

where ε_M is the electrolyte volume fraction of the membrane.

The Crank-Nicholson implicit method is used to evaluate the derivatives in time [13]. Solving for the mass balance and determining how much platinum dissolves, the cathode catalyst surface area as a function of time is obtained from (1).

4.1 Dissolution and Platinum Particle Growth

The dissolution of the platinum ions in the catalyst layer has been empirically observed to reduce the radius of small platinum particles and increase the radius of larger ones due to Ostwald ripening [13, 37]. The net result is an increase in radius of the particles (Figure 3 right) and decrease in catalyst surface area (Figure 3 left). This effect of increased particle radius increases available catalyst surface area; however platinum particles are also dissolved away resulting in an overall reduction catalyst surface area. The previous model from [13] captured these general trends but the model predicted rate of particle radius increase is substantially higher than experimental data, while catalyst surface decrease is smaller than the experimental data (Figure 3). This earlier model predicts a much higher rate in particle radius growth rate and lower decrease in electrochemical surface area. Thus, this previous model is expected to underestimate the rate of catalyst degradation than what the experimental data would suggest [13]. By accounting for particle migration, more of the dissolved

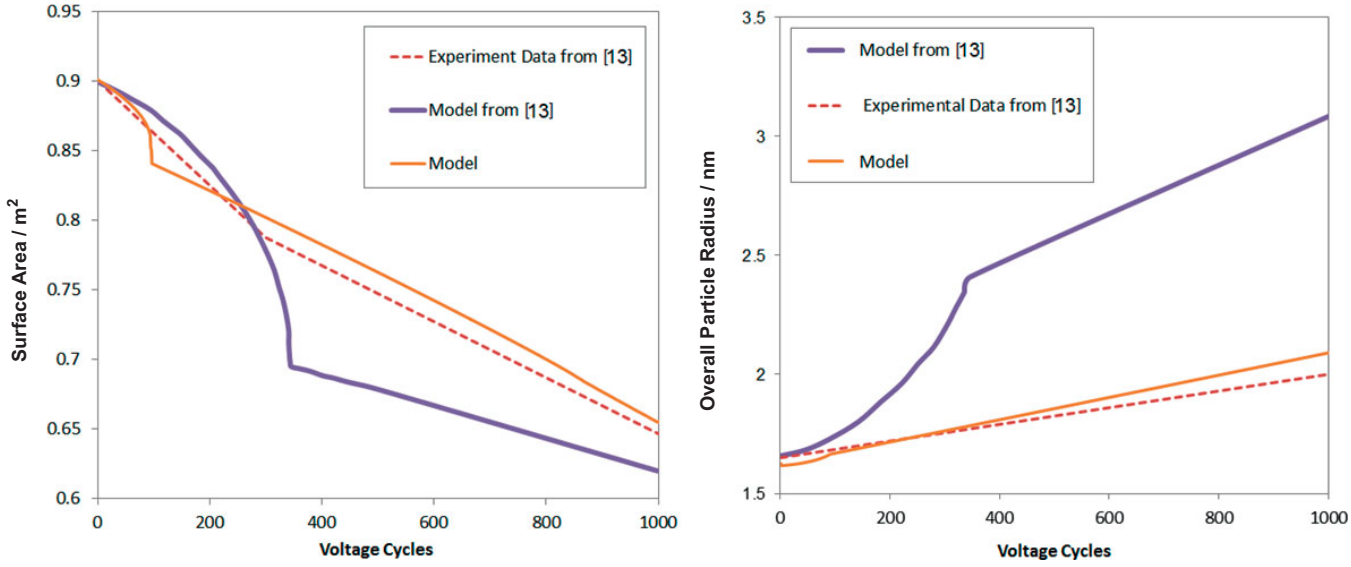

Fig. 3 (Left) Simulated and experimental cathode platinum catalyst surface area (Right) Overall Platinum Catalyst Particle Radius under voltage cycling (square wave – 0.87 to 1.2 V, period 60 s, Temperature 25 °C, cathode relative humidity 50%).

platinum particles are "washed away", without being able to deposit on large platinum particles and increase their radius. By accounting for migration, the effect of Ostwald ripening is reduced. This closely matches the observed drop in surface area, without a substantial increase in particle radius (Figure 3). Overall, the model presented here better matches the longer term rate of decrease of the catalyst surface area and rate of increase of particle radius than the previous model. This ability to well match several observable system parameters is critical for prediction of fuel cell catalyst life from the model.

4.2 Life Prediction

The rate of change in surface area of the catalyst particles is used to estimate the catalyst life of the fuel cell. Here, the effective end of the fuel cell catalyst life is assumed to occur when the catalyst surface area has decreased by 25% before any degradation ($S(t)/S_0 = 0.75$) a more stringent assumption than from [30]. This is value is chosen to operate the fuel cell within a linear degradation regime. Beyond 25% surface area degradation, it is expected that the impact on performance will be drastic and non-linear. The time, T for a fuel cell to reach this point is:

$$T = \frac{-S_0}{4\Omega} \tag{16}$$

where:

S_0 is the initial surface area

$\Omega = dS_0/dt$ and is the rate of catalyst surface area degradation.

4.3 Degradation of Polarization Curve and Power Output

The degradation in catalyst surface results in a decrease in voltage. This change in voltage $\Delta V(t)$ is calculated at the maximum power output voltage, V_{Pmax}:

$$\Delta V_{V_{\mathrm{Pmax}}}(t) = \upsilon \frac{S(t)}{S_0} \tag{17}$$

where:

$\Delta V_{V_{\mathrm{Pmax}}}(t)$ is the change in potential due to degradation at voltage V_{Pmax} and time t.

υ is the "slope" constant determined empirically from Figure 6 in [19], relating cell voltage losses to electrochemically active surface area (ECSA) loss.

$S(t)$ is the ECSA of the catalyst at time t.

S_0 is the initial surface area.

The behavior and performance of a fuel cell is observed using a polarization curve, a function that relates the device's output voltage to its current. The degraded polarization curve is obtained as a function of a polarization curve before any degradation:

$$V(t, V_0(i)) = \varphi(t) \ln[V_0(i)] + V_{\mathrm{OCV}} \tag{18}$$

where:

$V_0(i)$ is the voltage obtained for current i of a fuel cell before any degradation.

V_{OCV} is the open circuit voltage before any degradation.

The slope, $\phi(t)$:

$$\phi(t) = \frac{V_{\mathrm{Pmax}} + \Delta V_{V_{\mathrm{Pmax}}}(t) - V_{\mathrm{ref}}}{\ln(V_{\mathrm{Pmax}})} \tag{19}$$

where:

V_{Pmax} is the voltage at the maximum power output voltage.

t is time.

V_{ref} is a constant.

The effect of catalyst degradation on PEM fuel cells are shown in Figure 4 (left), a typical polarization curve of the fuel cell. The figure shows the polarization curve of a fuel cell at the beginning of its life, followed by the cell at 50% life and end of life (i.e. when $S(t)/S_0 = 0.75$). As a cell degrades, its voltage drops, reducing the output power shown in Figure 4 (right). The reduction in power output due to degradation is significant and increases for increased voltages as shown. It is also important to note that the peak power point shifts to lower operating voltages as the cell degrade.

5 Experimental Results

The objective of the experiments is to test the catalyst degradation model presented for fuel cells at critical operating points relevant to the field applications.

Since the desired life of the power supply for these devices is often in the 3–5 years, experimentally verifying the module for such long times is not feasible. Here, the degradation rates obtained from short term experiments of 1 week to 2 months is projected to support our long term predictions. The initial phase of catalyst degradation has been shown to be linear based on extensive experimental results [14, 15]. The physical phenomena captured in the model that affect the catalyst degradation are the dissolution of the platinum into ions and redisposition of platinum particles into larger ones, resulting in platinum particle growth [13]. These phenomena have been empirically found to reach steady state dissolution rates within 48 h and in the order of minutes for platinum particle growth rate [40, 13]. Hence, 1 week to 2 month experiments are sufficiently long to capture the impact of this phenomenon on fuel cell degradation.

A common approach to measuring catalyst degradation rates is to measure the voltage drop, for a given electrical load (resistance) and correct for these voltage drops by accounting for the change in membrane resistance. This procedure enables measuring the voltage drop due only to cathode catalyst degradation. A second approach uses cyclic voltammetry to measure the ECSA and compare this against the model predicted loss of platinum surface area. Other approaches are available such as measuring the loss of platinum but they require destructive disassembly of the fuel cell. Hence, these two methods were chosen.

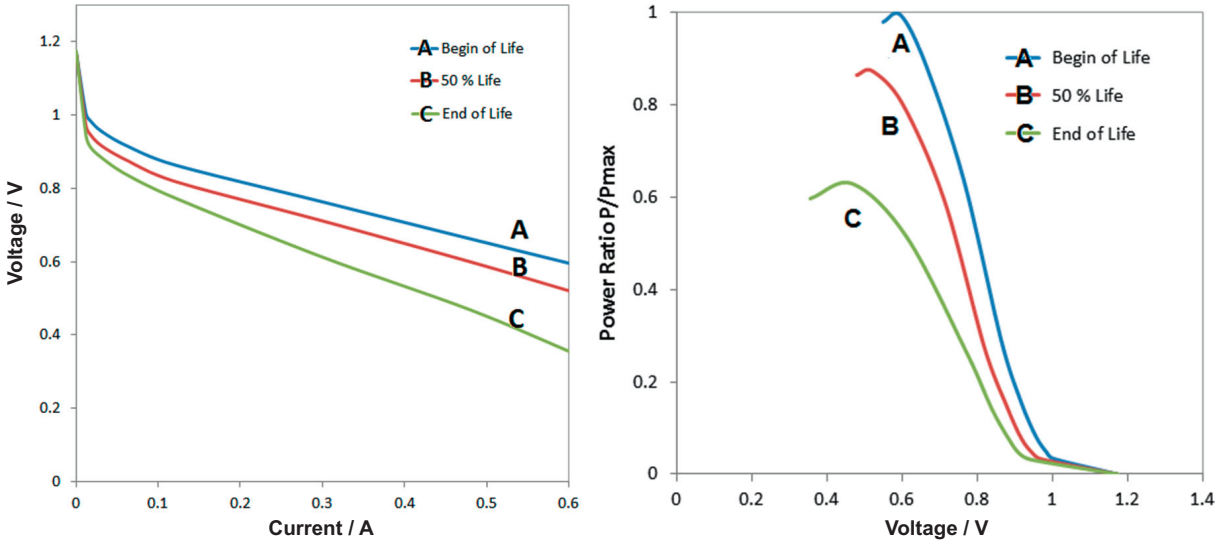

Fig. 4 Theoretical polarization curves displaying the relationship between voltage and current for a 6.7 cm^2 PEM fuel cell (Left) and power output (Right) of a fuel cell before and after degradation.

The key components of the experimental set-up are reactant gases, hydrogen, and air from high pressure tanks, a fuel cell test station (University Test Station, Fuel Cell Technologies, NM) and fuel cell block (from Fuel Cell Technologies) containing a MEA, a sandwiched combination of the GDL, membrane, and catalyst layers. The MEA is an air breathing cell from the FuelCellStore.com. The cell has an electrode area of 2.3 cm × 2.3 cm, a catalyst loading of 0.5 mg cm^{-2} and a Nafion 117 membrane. For the life experiments, the following procedure is followed. Each cell is initialized at nominal conditions:

- Hydrogen is fed at 10 SCCM (Standard Cubic Centimeters per Minute), at room temperature, 100% relative humidity,
- Air is fed at 500 SCCM and set at room temperature and at 50% relative humidity.
- The reference load, R_L is obtained from measuring the electrical load (resistance) of the fuel cell operating at 0.4 V.

For the experiments:

- Hydrogen is fed at 5 SCCM and air is fed at 500 SCCM at an experiment specified humidity and temperature.
- The operating voltage for the experiment is maintained by the fuel cell test station for 1 week.
- After each 24 h of operation at the experimental conditions, the fuel cell is set to the reference load, R_L.
- The fuel cell is set at the reference load for voltage degradation measurement because the effects of voltage degradation is magnified at lower voltages (Figure 4 left) and hence can be measured accurately.

Apart from voltage measurements, cyclic voltammetry is a well-established method used to measure the ECSA of the fuel cells before and after degradation. The measurements are performed using a VoltaLab PST050 (Radiometer Analytical, France) potentiostat at 20 mV s^{-1}, at 25 °C, with both anode and cathode fully humidified. The ECSA measurements start by feeding the anode with hydrogen at 50 SCCM and cathode (the electrode of interest) with nitrogen at 5 SCCM to perform hydrogen adsorption/deadsorption (HAD) [43, 45]. The nitrogen is fed at this low flow rate to minimize artifacts produced in the ECSA measurements [44]. A flow rate of 1 SCCM cm^{-2} MEA area had been found to minimize this effect [44]. Using these cyclic voltammetry readings and well established procedure to obtain catalyst area per catalyst loading, the change in ECSA values are obtained before and after the electrochemical surface area measurements.

The theoretical and observed rate of voltage degradation for the reference operating voltage of 0.4 V is shown in Table 1 for 10 operating conditions chosen relevant for field applications. The results also show the predicted and measured using ECSA measurements taken using cyclic voltammetry. The ECSA results show good correlation with the predicted results, although the observed change in ECSA is found to be slightly higher than predicted. Furthermore, as presented earlier, previous ECSA from [13] match well with the predicted surface area from the model shown in Figure 3 for different set of experimental conditions (left). These results confirm that the voltage degradation is due to surface area loss of the catalyst. All of these experimental results show an excellent match and support the model predicted rates of fuel cell cathode catalyst degradation.

6 Model Analysis

6.1 *Effect of Migration*

This model of catalyst degradation differs from previous models due mainly to inclusion of migration in catalyst dissolution. In this section, the effect of migration is analyzed for relevant operating conditions. Figure 5 shows the effect of

Table 1 Voltage degradation rates from experiments.

Operating condition	Operating voltage (V)	Time (h)	Environment condition	ECSA		Model predicted rate of voltage degradation (V h^{-1})	Observed rate of voltage degradation (V h^{-1})
				Model (% change)	Measured (% change)		
1	1.0–0.75	168	15–40 °C, RH 15–75%	–14%	–16%	1.3×10^{-4}	1.5×10^{-4}
2	0.8	168	15–40 °C, RH 15–75%	> –1%	> –1%	2.5×10^{-5}	2.7×10^{-5}
3	0.8	168	20–25 °C, RH 30–50%	> –1%	> –1%	1.9×10^{-5}	2.0×10^{-5}
4	0.95–0.88	168	25 °C, RH 80%	–27%	–29%	6.6×10^{-4}	6.7×10^{-4}
5	0.8	168	25 °C, RH 80%	> –1%	–1%	2.2×10^{-5}	2.4×10^{-5}
6	0.8–0.7	168	25 °C, RH 30–50%	> –1%	> –1%	2.1×10^{-5}	1.8×10^{-5}
7	0.8–0.9	168	25 °C, RH 50%	–2%	–5%	3.8×10^{-5}	4.2×10^{-5}
8	0.94–0.83	168	25 °C, RH 50%	–6%	–7%	2.0×10^{-4}	2.1×10^{-4}
9	0.73–0.75	1400	20–25 °C, RH 30–50%	> –1%	0%	2.0×10^{-6}	$<2.0 \times 10^{-6}$
10	0.82	2160	20–25 °C, RH 30–50%	–5.5%	–6%	4.2×10^{-5}	4.4×10^{-5}

introducing migration into the catalyst degradation model. In particular, this effect is dependent on the electric field. For high voltages, beyond 0.87 V there is low current and hence the effect of migration is negligible as had been explained in [13]. However for a typical PEM fuel cell (see Figure 4 left for the model polarization curve), the voltage needs to be lower to produce sufficient power. For voltages between 0.75 and 0.85 V, the effect of migration on the total life of the fuel cell is substantial with a 30–40% reduction in life (respectively). This confirms our earlier assertion that this phenomenon cannot be ignored.

Advancement in fuel cells has resulted in increased current density. These results suggests, that increased current density (resulting in stronger electric field) particularly in the voltage range of 0.85 and 0.75 V can decrease the life of the fuel cell noticeably. The results show the life can further increased by reducing the current density. It should be noted that for lower voltages, the effect of catalyst dissolution is limited and hence the contribution of catalyst migration on the overall life is not expected have a practical impact (as shown in Section 6.1).

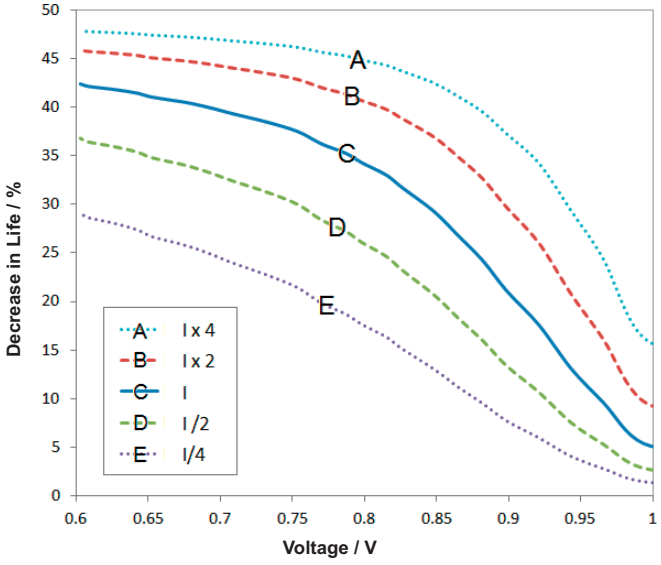

Fig. 5 Percentage decrease in life by incorporating migration into the catalyst degradation model for nominal current density I. The effect of increased and decreased current density (I) on life due to catalyst migration is also shown.

6.2 Operating Voltage

The effect of operating voltage on PEM fuel cells predicted by the model can be seen from Figure 6, where the life of the fuel cell catalyst exponentially decreases with increased operating voltage. Increased operating voltage has been shown to produce higher operating efficiency thus requiring less fuel [23]. The operating voltage chosen for a fuel cell application requires careful consideration of these conflicting factors.

6.3 Voltage Fluctuations

A typical power profile of all but the simplest electrical devices will have varying electrical loads, resulting in voltage fluctuations. Voltage fluctuations can also be caused by electrical noise in a system. Figure 7 shows the effect of voltage fluctuation on the percentage reduction of fuel cell catalyst life. For this plot, the fluctuation effects are obtained by comparing the catalyst life of the fuel cell oscillating in a square wave between a voltage say 0.8 and 0.9 V and when held constant at the average voltage of 0.85 V. The results show the reduction in catalyst life increases linearly with increasing amplitude.

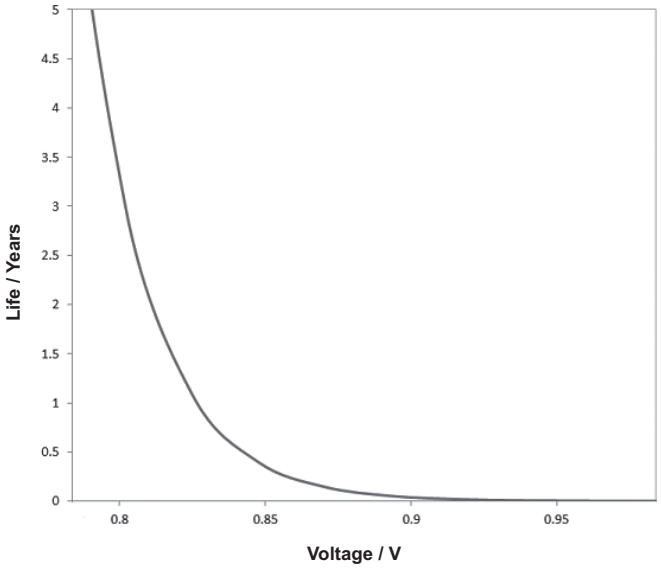

Fig. 6 The predicted effects of operating voltage on a fuel cell catalyst life (cathode humidity 50%, temperature 25 °C).

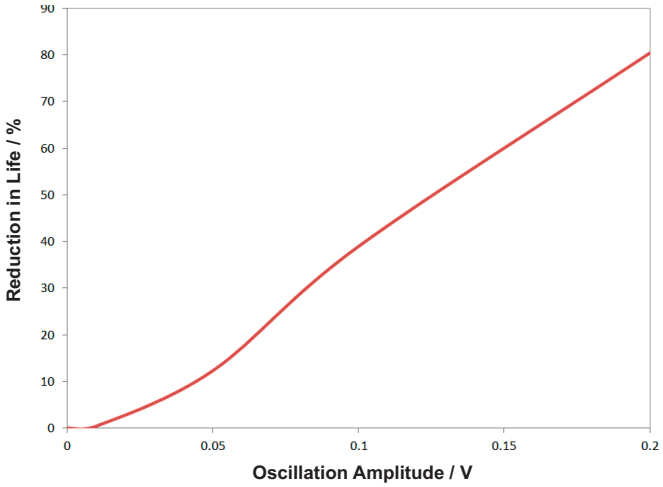

Fig. 7 The predicted effect of voltage fluctuation on catalyst life (voltage 0.8 V, square wave, 0.17 Hz, temperature 25 °C, cathode relative humidity 50%).

To understand the full impact of voltage oscillations, the percentage reduction in life value needs to be multiplied to the expected life in Figure 6 to obtain an absolute effect on life. The results show that operating voltage is the dominant factor compared to voltage oscillations; however at high oscillating amplitudes the effects are substantial and cannot be ignored. Voltage fluctuation can accelerate degradation and is mentioned in earlier experimental evidence [13, 37]. However in this study, the effect of voltage fluctuation is isolated from the effect of operating at a high voltage even when oscillating in a square wave. This enables us to identify the effect of voltage oscillation amplitude alone on catalyst degradation and life. This predicted decrease in catalyst life can be explained from the process of platinum oxidation. Platinum oxide films readily form at high voltages and protect the platinum particles underneath it from further dissolution. In addition, these oxide films disappear at low voltage. This momentary transition from a low voltage, where there is little oxide filming to a high voltage makes the platinum particles vulnerable, where the platinum oxide films have not formed fast enough to protect the platinum particles from the higher voltage hence this results in momentary accelerated dissolution of platinum particles. These brief instances are sufficient to have a noticeable impact on life because of the very high rate of platinum dissolution at voltages above 0.8 V. A typical power profile of all but the simplest electrical devices will have varying electrical loads and impart electrical noise resulting in voltage fluctuations. As will be discussed later in Section 7.2, the effect of noise and load variation can be mitigated by using the fuel cells in a hybrid configuration a small battery and appropriate filters.

6.4 Temperature

The effect of temperature on fuel cell performance is critical for field devices, where temperatures will vary over the course of a day and seasonally. The effect of temperature on fuel cell catalyst life is shown in Figure 8. For increased temperature, an exponential decrease in life is predicted by the model. For example, operating at 0.8 V the life is 4.5 times shorter operating at 60 °C than for 15 °C. Low temperatures decreases catalyst degradation and increasing life, but can produce other problems such as increased condensation resulting in flooding. While it is well understood that flooding does not affect the life of the fuel cell, it can result in significant losses of power output. In conclusion, it is important to design and control the temperature of a fuel cell to maximize life.

6.5 Humidity

Humidity is also an important operating parameter for fuel cell catalyst life. The effect of cathode humidity on the catalyst life of an air breathing PEM fuel cell is shown in Figure 9. As seen, life is significantly shortened when the relative humidity approaches 0, while a peak occurs at 10% relative humidity. Further increase in humidity is less substantial.

This result is caused by varying rate of platinum oxide formation due to cathode humidity. The platinum oxide formation reaction (3) requires water and at low cathode humidity, this reaction is starved of water and as a result does not form a protective film to prevent dissolution of platinum. At slightly higher humidity, the reaction obtains sufficient water and minimal impact from proton activity (see Eq. 5). This enables the system to achieve a maximum in terms of life, because oxidation helps protect the platinum from further dissolution and there is limited impact from proton activity. However, with further increase in humidity, the proton activity due to the electric field increases and this acts as a resistance factor in the formation of platinum oxide (Eq. 5). Similar to the issue of low temperature, high humidity can cause

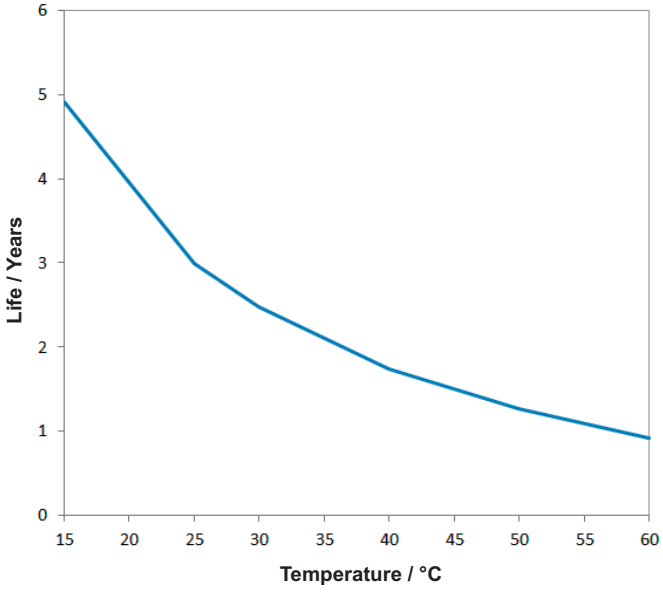

Fig. 8 The predicted effect of temperature (Voltage 0.8 V, cathode relative humidity 50%).

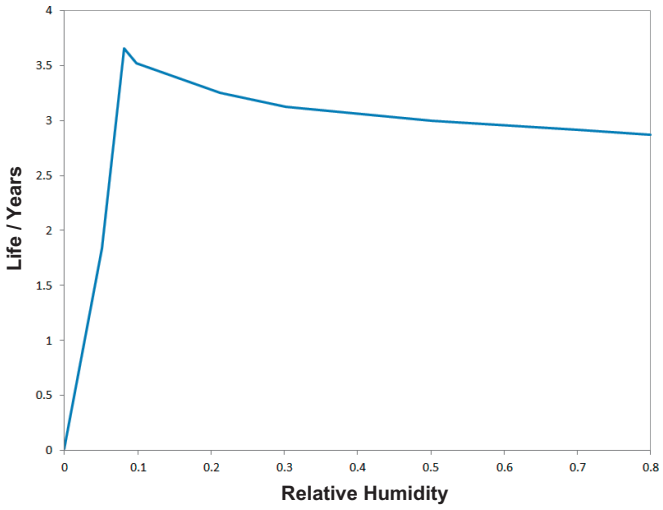

Fig. 9 The predicted effect of cathode relative humidity on fuel cell life (voltage 0.8 V, temperature 25 °C).

flooding resulting in drastic loss in output power. Recently, developed self-humidifying PEMs may alleviate this problem by ensuring the gas streams are not too dry.

In summary, based on the models, operating voltage has exponential influence on fuel cell life, followed by operating temperature. Low humidity has significant influence on catalyst degradation, but high humidity is found to have limited effect on catalyst life. Voltage fluctuation is found to have linear influence on fuel cell catalyst life. As discussed in the following sections, these factors need to be considered in the design of fuel cell powered field devices.

6.6 Operating Parameters for Long Life

The effects of operating conditions on fuel cell degradation have been extensively studied. However, here a physical model is being used to quantify these different effects into predicted life. The predicted life is a proposed metric that can be used to quantify the relative importance and effect of field conditions on the catalyst particularly in the design and control of fuel cell power supplies. This permits the results of these studies to be analyzed and system design or control trade-offs be performed to best meet life and performance requirements of the fuel cell power supplies for specific practical applications.

The above results highlight the fragility and short life of fuel cell catalyst under certain conditions, these results also show that fuel cells can be operated within an operating window to minimize degradation and maximize life. This can be accomplished through effective control and judicious design choices. A set of practical operating parameters and general guidelines is shown in Table 2 and is expected to achieve 2 or more years of catalyst life.

Operating at a voltage of 0.8 V is expected to substantially reduce the effects of catalyst degradation and translates into operating efficiency (conversion from chemical to electrical) of ≤65% (LHV) [23]. This result matches earlier experimental finding that suggest catalyst degradation is substantially lower below 0.8 V [37]. Furthermore, catalyst degradation can be minimized by lowering the temperature. A temperature range of 15–35 °C is practical for a typical small, air breathing fuel cell. A relative humidity of higher than 10% and <80% is expected to minimize the effects of humidity on degradation but this needs to be carefully considered, in terms of water management for a specific fuel cell design to avoid flooding and drying.

Table 2 PEM fuel cell operating conditions to maximize catalyst life and operating efficiency.

Operating variable	Value
Voltage	≤ 0.8 V
Temperature	15–35 °C
Cathode relative humidity	10% < RH ≤ 80%

7 Case Studies

Here, the use of fuel cell power supplies for a representative application is considered, namely a field sensor module.

7.1 Field Sensor Network Module

Networks of field sensor modules have potential for remote border protection, environmental monitoring, and exploration [21, 35]. These devices ideally need to operate for 3–5 years or more. Such modules may contain temperature, humidity/moisture, vibration, accelerometers, chemical, and light sensors. Their data may periodically be transmitted to a base station. Hence, they will typically be low power devices that operate intermittently at higher power over long periods.

Their data may periodically be transmitted to a base station. Here, a buried sensor might detect the presence of intruders [31]. Sensor can also be mobile, equipped with a polymer actuator to hop, roll, and bounce, exploring rugged terrains and caves [35]. Consider a sensor module as shown in Figure 10. It consists of a power supply, an accelerometer to detect vibration, electronics to interface with the sensor, a

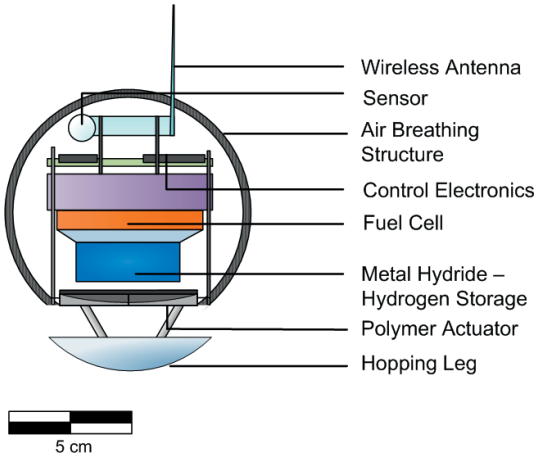

Fig. 10 A Field sensor module.

wireless radio for communication, and polymer dielectric elastomer actuator (DEA) for hopping [42]. The hopping mechanism is light weight and compact, weighing in the order of tens of grams and consumes 50% of total energy required by the sensor module. Figure 11 shows the assumed sensor module power demand curve. It shows 50 mW average, 100 mW peak at a 0.5 duty cycle. The total mass of the module is assumed to be 1.5 times the mass of the power system.

It is assumed that the field sensor is deployed in a desert location, operating continuously, where temperature varies between 15 and 40 °C (Figure 12 left) and humidity varies between 0.15 and 0.75 (Figure 12 right).

First batteries are considered as power supplies for these sensors. Batteries exhibit self-discharge where stored energy is lost at a fixed rate modeled as a geometric series. Also, it is assumed that the last 20% of the energy that cannot be used. The mass of a battery power supply required is:

$$M_{\text{bat}} = \frac{a\rho_{\text{bat}}E(T)\left(1-r^{T}\right)}{1-r} \tag{19'}$$

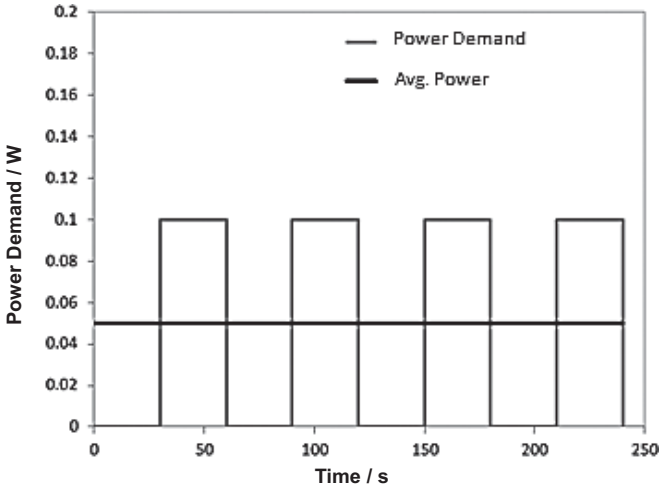

Fig. 11 Power demand curve for the field sensor.

where

M_{bat} is the total mass of the battery power supply required for T years of life.

a is the capacity margin.

r is the self-discharge rate.

ρ_{bat} is the energy density of the battery.

$E(T)$ is the energy required to power a payload device for T years according to a given duty cycle.

The energy densities, self-discharge rates, and mass of the battery power supplies are shown in Table 4.

The mass of a PEM fuel cell power supply for this case is given by:

$$M_{\text{fuel}} = \frac{\rho_{\text{fuel}}E(T)}{r} \cdot \ln\left|\frac{0.5-\frac{1}{r}}{T+0.5-\frac{1}{r}}\right| \tag{20}$$

where

M_{fuel} is the total mass of the fuel for T years of life.

ρ_{bat} is the energy density of the fuel.

$E(T)$ is the energy required to power a payload device for T years for a given a power profile.

$r = \mathrm{d}P/\mathrm{d}t$ is the power degradation rate of the fuel cell power supply for a specified operating point.

The mass calculated accounts for the extra fuel required due to losses from degradation and to ensure that fuel cell provides the energy required at the end of T years. Table 3 shows the mass breakdown of the fuel cell power supply. The power supply consists of the fuel cell, lithium hydride fuel storage, electronics and other components. The lithium hydride fuel produces hydrogen with the addition of water generated from the fuel cell or extracted passively from the air [13, 36].

7.2 Comparison between Batteries and Fuel Cells

The performance of a battery and the PEM fuel cell power supply for field sensor modules are compared in Table 4. Rechargeable batteries such as lithium ion are substantially heavier owing to their high rate of self-discharge. The non-rechargeable batteries such as the Alkalines fare better, although they have a low energy density. Other non-recharge-

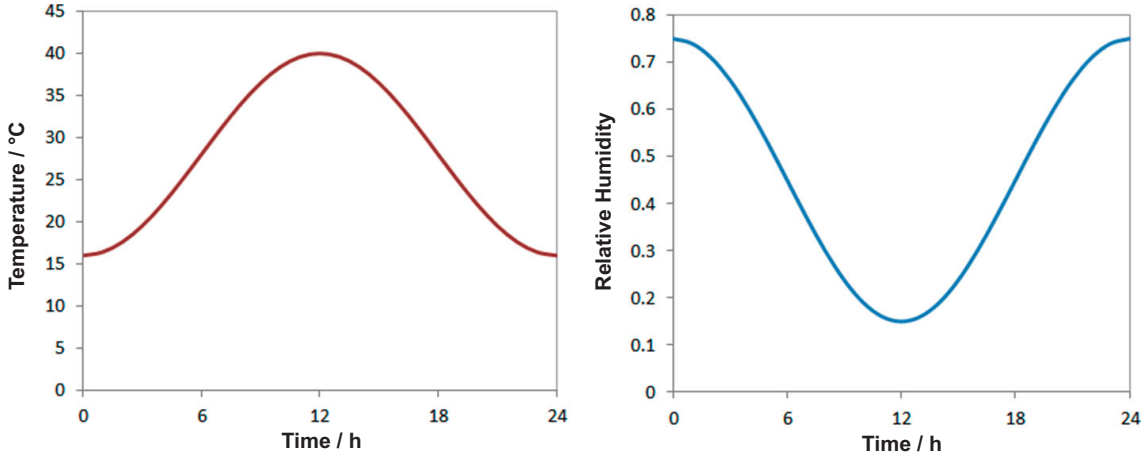

Fig. 12 Model of daily temperature profile (Left) and relative humidity (Right).

able batteries particularly the Lithium CR and lithium thionyl chloride batteries have relatively high energy density and even lower rates of self-discharge.

Operating the PEM fuel cells at 65% conversion efficiency (LHV) results in higher rates of degradation causing loss of power and the using of high energy density fuel such as lithium hydride that is not prone to self-discharge, the system is nearly 10 fold lighter than the best batteries (Table 4). A sensor module weighing a few kilograms or more lacks scalability to hundreds or thousands of modules owing to high cost and logistics required for deploying them.

Assume in this scenario that 50% of the energy consumed by the sensor is used for hopping and that the sensor module hops at a 45° angle, with an initial velocity of 2 m s^{-1} and maximum height of 0.1 m to yielding 0.41 m distance traversed per hop. The electrical energy, E_{hop} required per hop (neglecting air resistance) is the following:

$$E_{hop} = \frac{1}{2\eta_{EM}} mv^2 \tag{21}$$

where

η_{EM} is the electrical to mobility efficiency of the DEA hopping mechanism and is 13% [35, 42].

m is the mass of the sensor module.

v is the initial velocity of the sensor module.

The maximum range, l per hop is then:

$$l = \frac{v^2}{g} \sin 2\theta \tag{21'}$$

where

v is the initial velocity of the sensor module.

g is the gravitational acceleration and is 9.8 m s^{-2}

θ is the hopping angle and is 45°

Savings in mass can be significant if the sensor module needs to be mobile (i.e. hop) as shown in Table 5. Battery powered sensor modules, particularly using alkalines, lithium ion, and lithium CR batteries have very short range owing to their high mass. Lithium thionyl chloride batteries have the greatest range of the all the batteries compared but have nearly 10-folds shorter range than the proposed fuel cell power supply. These results show that a fuel cell has the potential to be light weight and efficient power source for sensor modules.

Table 3 Mass breakdown of fuel cell power supply for sensor network module (3 years life).

Component	Mass (kg)
Fuel cell	0.01
Lithium hydride fuel + storage	0.36
Electronics	0.10
Other components	0.20
Total	0.40

7.3 Long Life

As discussed earlier, while fuel cells have the potential to be a superior, light weight, efficient power replacement to batteries, they are faced with limited durability and short life. In this section using the model developed in this paper, several fuel cell power supply configuration are considered to maximize catalyst life and reliability. For this analysis, it is assumed the fuel cell during its life avoids flooding, drying, and fuel or oxygen starvation. Several fuel cell power supply configuration are considered. Figure 14 shows a fuel cell power supply connected directly to a sensor load. Figure 13 shows the fuel cell power supply connected in a fuel cell battery hybrid configuration, with noise suppression circuitry [27] but without environmental controls. In the hybrid configuration, the fuel cell operates at fixed voltage and trickle charges a battery that handles the varying power demands of the load protecting the fuel cell from varying power demands and electrical noise. Figure 14 shows the hybrid configuration combined with a fuel cell environmental control system. Table 6 shows the parameters used for each configuration and expected fuel cell catalyst life. The last column shows the predicted life of the fuel cell catalyst based on experimental degradation rates of operating conditions 1 through 3 presented in Table 1. The fuel cell connected directly to the sensor load has a life of only a few months because of the varying operating voltage. For the given operational duty cycle (Figure 11), the fuel cell switches between 1.0 and 0.75 V, producing 0 and 100 mW, respectively from Figure 4.

The operating voltage has an exponential effect on fuel cell catalyst life as seen from Figure 6, while voltage oscillation has a linear effect (Figure 7). To reduce the effects of degradation, the fuel cell is held at fixed operating voltage (0.8 V) using a hybrid configuration, where the battery supplies peak power, while the fuel cell trickle charges the battery [28]. A sevenfold improvement in life is predicted by the model as shown in Table 6 and this is confirmed by the experimental results. A further 30% improvement in life can be obtained by adding environmental controls to the hybrid system (Figure 14). With environmental controls, the fuel cell is operated within a range of temperature and humidity to give long life. It should be noted that these prediction assume that the effect of fuel cell (cathode) catalyst degradation is the dominant factor that cause fuel cell degradation.

Table 4 Power supply comparison for 3 years life.

Power supply	Energy density (Wh $\cdot kg^{-1}$)	Self-discharge/degradation per month (%)	Mass (kg) (3 years Life)
Alkaline	110	0.5	15.6
Lithium ion	140	5	33
Lithium manganese dioxide	270	0.17	6
Lithium thionyl chloride	420	0.08	3.8
Fuel cell using lithium hydride (65 eff.%, 25 wt.% H_2) [22, 36]	4,900	1.2	0.4

Table 5 Power supply and range of mobile sensor.

Power supply	Mass (kg) (3 years life)	Number of hops	Range (km)
Alkaline	15.6	6,600	2.7
Lithium ion	33	3,100	1.3
Lithium manganese dioxide	6	17,000	7.1
Lithium thionyl chloride	3.8	27,000	11
Fuel cell using lithium hydride (65 eff.%, 25 wt.% H_2) [22, 36]	0.4	260,000	104

8 Conclusion

In this paper, catalyst degradation is identified as an important cause of PEM fuel cell unreliability and short life. An experimentally tested model of this degradation is presented that predicts the catalyst life of a PEM fuel cell and its power output. The model accounts for the effects of degradation due to particle migration and dissolution. The effect of particle migration had been ignored in previous models. However in the work, it is found that particle migration can have a substantial effect on catalyst degradation and thus cannot be ignored. Accounting for particle migration, the model better matches previous experimental data and permits longer term prediction of fuel cell life and performance. The model is used to quantify and make life-time predictions under varying power demands, temperature, and humidity. The predicted life is a proposed metric that can be used to quantify the relative importance and effect of field conditions on the catalyst particularly in the design and control of fuel cell power supplies. This model is applied to predict the life and performance of PEM fuel cells for powering a field sensor module. The case study shows that PEM fuel cells would be far superior to batteries in terms of mission duration and energy density. The model predicted results supported by experimental evidence show that long-lives can be achieved with PEM fuel cells connected in a hybrid configuration with a battery, a power conditioning circuitry, and environmental control system to maintain acceptable temperature and humidity. This protects the fuel cell from premature failure caused by degradation leading to long operational lives. Current research is focusing on passive methods to maintain ideal fuel cell operating conditions to achieve long lives.

Acknowledgements

The support for this work by Israel's MAFAT Basic Science Office of the MOD is gratefully acknowledged as is the contributions of Igal Klein, Alex Schechter, Yang Shao Horn, Kavya Kamal Manyapu, Daniele Gallardo, Daniel Strawser, and Ling Ling Deng. Jekanthan Thangavelautham was partly supported by NSERC Canada.

Appendix: List of Constant and Their Values

Variable	Value
C_0	0.043
C_1	17.81
C_2	–39.85
C_3	36
C_4	1.98
C_5	0.0324
C_6	0.0648
k_a	181.6
k_b	0.03
k_c	0.062
k_d	0.634
k_e	3
κ_0	10
κ	13.3
β	4.18

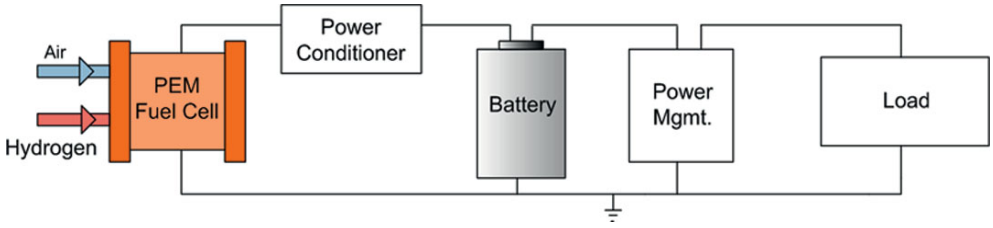

Fig. 13 PEM fuel cell in a hybrid configuration, where fuel cell output a constant power that is used to trickle charge a battery.

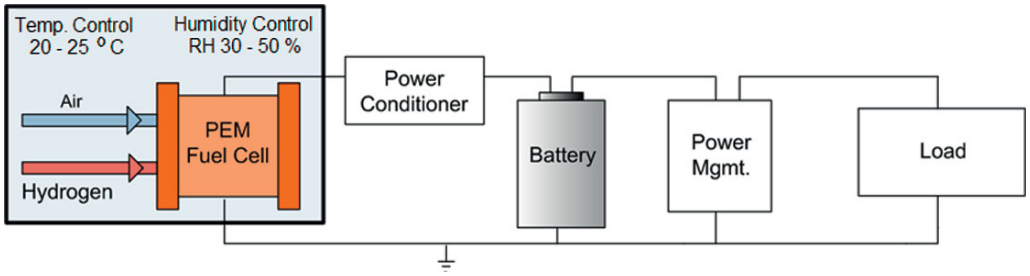

Fig. 14 PEM fuel cell in a hybrid configuration, with the fuel cell operating under environment control that maintains humidity and temperature at desired conditions.

Table 6 Fuel cell power supply configurations for a field sensor.

Fuel cell system configuration	Operating voltage (V)	Power output (W)	Fuel cell environment control	Life (months) predicted from simulation degradation rates	Life (months)predicted from experiment degradation rates
Fuel cell direct	1.0–0.75	0.003–1.0	15–40 °C, RH 15–75%	4.3	5
Fuel cell hybrid + power conditioning	0.8	0.05	15–40 °C, RH 15–75%	30	28
Fuel cell hybrid + power conditioning + environment control	0.8	0.05	20–25 °C, RH 30–50%	40	39

References

[1] A. Collier, H. Wang, X. Yuan, J. Zhang, D. P. Wilkinson, *Int. J. Hydrogen Energy* **2006**, *31*, 1838.

[2] A. B. LaConti, M. Hamdan, R. C. McDonald, in: W. Vielstich, H.A. Gasteiger, A. Lamm (Eds.), *Handbook of Fuel Cells: Fundamentals Technology and Applications 3*, John Wiley & Sons Ltd., Hoboken, NY, USA, **2003**, p. 647.

[3] J. Wu, X. Z. Yuan, J. J. Martin, H. Wang, J. Zhang, J. Shen, S. Wu, W. Merida, *J. Power Sources* **2008**, *184*, 104.

[4] X. Huang, R. Solasi, Y. Zou, M. Feshler, K. Reifsnider, D. Condit, S. Burlatsky, T. Madden, *J. Polym. Sci.* **2006**, *16*, 2346.

[5] C. Yang, S. Srinivasan, A. B. Bocarsly, S. Tulyani, J. B. Benziger, *J. Membr. Sci.* **2004**, *237*, 145.

[6] T. Akita, A. Taniguchi, J. Maekawa, Z. Siroma, K. Tanaka, M. Kohyama, K. Yasuda, *J. Power Sources* **2006**, *159*, 461.

[7] S. Y. Ahn, S. J. Shih, H. Y. Ha, S. A. Hong, Y. C. Lee, T. W. Lim, I. H. Oh, *J. Power Sources***2002**, *106*, 295.

[8] S. D. Knights, K. M. Colbow, J. St-Pierre, D. P. Wilkinson, *J. Power Sources* **2004**, *127*, 127.

[9] M. A. Rubio, A. Urquia, S. Dormida, *Int. J. Hydrogen Energy* **2010**, *35*, 1.

[10] E. A. Cho, J. J. Ko, H. Y. Ha, S. A. Hong, K. Y. Lee, T. W. Lim, I. H. Oh, *J. Electrochem. Soc.* **2004**, *151*, A661.

[11] Y. Shao, G. Yin, Y. Gao, *J. Power Sources* **2007**, *171*, 558.

[12] J. Hou, H. Yu, S. Zhang, S. Sun, H. Wang, B. Yi, P. Ming, *J. Power Sources* **2006**, *162*, 513.

[13] W. Bi, T. F. Fuller, *J. Power Sources* **2008**, *178*, 188.

[14] R. M. Darling, J. M. Meyers, *J. Electrochem. Soc.* **2003**, *150*, A1523.

[15] M. W. Fowler, R. F. Mann, J. C. Amphlett, B. A. Peppley, P. A. Roberge, *J. Power Sources* **2002**, *106*, 274.

[16] X. Cheng, Z. Shi, N. Glass, L. Zhang, J. Zhang, D. Song, Z. Liu, H. Wang, J. Shen, *J. Power Sources* **2007**, *165*, 739.

[17] J. Frisk, W. Boand, M. Hicks, M. Kurkowski, R. Atanasoski, A. Schmoeckel, *MEA Component Durability*, 2004 Fuel Cell Seminar San Antonio, TX, USA, November 1–5, **2004**.

[18] M. Inaba, T. Kinumoto, M. Kiriake, R. Umebayashi, A. Tasaka, Z. Ogumi, *Electrochim. Acta* **2006**, *51*, 5746.

[19] W. Bi, T. F. Fuller, *J. Electrochem. Soc.* **2008**, *155*, 215.

[20] C. Spiegel, *PEM Fuel Cell Modeling and Simulation Using Matlab*, Elsevier Academic Press, Waltham, Massachusetts, USA, **2008**.

[21] I. Akyildiz, W. Su, Y. Sankasubramanium, E. Cayirci, *IEEE Commun. Mag.* **2002**, *49*, 102.

[22] J. Thangavelautham, D. Strawser, M. Cheung, S. Dubowsky, Lithium Hydride Powered PEM Fuel Cells for Long-Duration Mobile Robotic Missions, Proceedings of the IEEE International Conference on Robotics and Automation (ICRA 2012), **2012**, pp. 415.

[23] F. Barbir, *PEM Fuel Cells: Theory and Practice*, Academic Press, Waltham, Massachusetts, USA, **2005**.

[24] R. O'Hayre, S. Cha, W. Colella, F.B. Prinz, *Fuel Cell Fundamentals*, Wiley, New York, NY, USA, **2005**.

[25] A. G. Ritchie, *J. Power Sources* **2005**, *136*, 285.

[26] P. Corke, P. Valencia, P. Sikka, T. Wark, L. Overs, *Long-Duration Solar-powered Wireless Sensor Networks*, Proceedings of the EMNets, June **2007**.

[27] D. Gallardo, *Power Management for Micro PEM Fuel Cells*, MS Dissertation, Mechanical Engineering Department, Politecnico di Torino, Torino, Italy, **2010**.

[28] J. Thangavelautham, D. Gallardo, D. Strawser, S. Dubowsky, Hybrid Fuel Cells Power for Long Duration Robot Missions in Field Environments, Proceedings of the 14th International Conference on Climbing and Walking Robots (CLAWAR), **2011**.

[29] I. F. Akyildiz, W. Su, Y. Sankarasubramaniam, E. Cayirci, *Comput. Netw.* **2002**, *38*, 393.

[30] DOE Cell Component Accelerated Stress Test Protocols for PEM Fuel Cells, Technical Report, US Department of Energy, **2007**.

[31] K. Manyapu, Feasibility Study of Long-Life Micro Fuel Cell Power Supply for Sensor Networks for Space and Terrestrial Applications, *Master's Thesis*, MIT Press, Cambridge, MA, USA, **2010**.

[32] A. Taro, M. Takasi, T. Satoshi, Y. Hiroshi, H. Tadahiro, H. Akira, H. Katsuo, T. Toshihiro, Y. Kazushisa, PEFC Deep Cruising AUV URASHIMA, Fuel Cell Symposium Proceedings, **2003**, pp. 90.

[33] H.-I. Joh, T. J. Ha, S. Y. Hwang, J.-H. Kim, S.-H. Chae, J. H. Cho, J. Prabhuram, S.lK. Kim, T.-H. Lim, B.-K. Cho, J.-H. Oh, S. H. Moon, H. Y. Ha, *J. Power Sources* **2010**, *195*, 293.

[34] S.-Y. Lee, I.-G. Min, H.-J. Kim, S. W. Nam, J. Lee, S. J. Kim, J. H. Jang, E. A. Cho, K. H. Song, S.-A. Hong, T.-H. Lim, *J. Fuel Cell Sci. Technol.* **2010**, 7, 0310061.

[35] S. B. Kesner, J. S. Plante, P. Boston, T. Fabian, S. Dubowsky, Mobility and Power Feasibility of a Microbot Team System for Extraterrestrial Cave Exploration, Proceed-

ings of the 2007 IEEE International Conference Robotics and Automation, Rome, Italy, April **2007**.

[36] J. Thangavelautham, S. Dubowsky, D. Strawser, Long-Life High-Energy Fuel Cell Power for Robots and Sensor Networks in Environmental Monitoring, Proceedings of the IROS 2011 Workshop on Robotics for Environmental Monitoring, p. 120.

[37] Y. Shao-Horn, W. C. Sheng, S. Chen, P. J. Ferreira, E. F. Holby, D. Morgan, *Top. Catal.* **2007**, *46*, 285.

[38] M. Pourbaix, *Atlas of Electrochemical Equilibria in Aqueous Solutions*, Pergamon Press, Oxford, United Kingdom, **1966**.

[39] P. J. Ferreira, G. J. La, Y. Shao-Horn, D. Morgan, R. Makharia, S. Kocha, H. A. Gasteiger, *J. Electrochem. Soc.* **2005**, *152*, A2256.

[40] X. Wang, R. Kumar, D. J. Myersz, *Electrochem. Solid State Lett.* **2006**, *9*, A225.

[41] L. Schlapbach, A. Zuettel, *Nature* **2001**, *414*.

[42] J. S. Plante, M. Santer, S. Pellegrino, S. Dubowsky, Compliant Bistable Dielectric Elastomer Actuators for Binary Mechatronic Systems, in Proc. of the ASME Conference on Mechanisms and Robotics, Long Beach, CA, USA, **2005**.

[43] J. Bett, K. Kinoshita, K. Routsis, P. Stonehart, *J. Catal.* **1973**, *29*, 160.

[44] R. N. Carter, S. S. Kocha, F. T. Wagner, M. Fay, H. A. Gasteiger, *ECS Trans.* **2007**, 11 403.

[45] M. Wesselmark, C. Lagergren, G. Lindbergh, *Electrochem. Soc. Trans.* **2009**, *25*, 1241.

[46] T. Madden, M. Perry, L. Protsailo, M. Gummalla, S. Burlatsky, N. Cipollini, S. Motupally, J. Jarvi, *Handbook of Fuel Cells – Fundamentals, Technology and Applications*, John Wiley & Sons, Hoboken, NY, USA, **2010**.

